GFTSM-based Model Predictive Torque Control for PMSM Drive System with Single Phase Current Sensor

Qingfang Teng, Yuxing Jin, Shuyuan Li, Jianguo Zhu, Youguang Guo

***Abstract*—A global fast terminal sliding mode (GFTSM)-based model predictive torque control (MPTC) strategy is developed for permanent magnet synchronous motor (PMSM) drive system with only one phase current sensor. Generally two phase-current sensors are indispensable for MPTC. In response to only one phase current sensor available and the stator resistance change, a novel adaptive observer for estimating both the remaining two phase currents and time-varying stator resistance is proposed to perform MPTC. Moreover, in view of the variation of system parameters and external disturbance, a new GFTSM-based speed regulator is synthesized to enhance the drive system robustness. In this paper, the GFTSM, based on sliding mode theory, employs the fast terminal sliding mode in both the reaching stage and the sliding stage. The resultant GFTSM-based MPTC PMSM drive system with single phase current sensor has excellent dynamical performance very close to the GFTSM-based MPTC PMSM drive system with two-phase current sensors. On the other hand, compared with PI-based and SM-based MPTC PMSM drive systems, it possesses better dynamical response and stronger robustness as well as smaller THD index of three-phase stator currents in the presence of variation of load torque. The simulation results validate the feasibility and effectiveness of the proposed scheme.**

NOMENCLATURE

R_s	Nominal phase resistance
ψ_m	The permanent magnet flux
ψ_s	Stator flux linkage
p	Number of pole pairs
V_{dc}	DC bus voltage
ω_r	Rotor actual mechanical speed
T_l	Load torque
T_e	Electromagnetic torque
J	Moment of inertia
B_m	Viscous friction coefficient
T_f	Coulomb friction torque
θ	Rotor electrical angular position
i	Stator current
u	Stator voltage
L	Stator inductance

I. INTRODUCTION

For PMSM drive system, the measurement of instantaneous stator currents is required for successful operation of the feedback control. Generally two phase current sensors are installed in three phase voltage source inverters (VSI). Nevertheless, sudden severe failure of phase current sensors would result in over-current malfunction of the drive system. And if there is no protection scheme in the gate-drive circuit, the failure would lead to irrecoverable fault of power semiconductors in VSI, which would cause degradation of motor drive performance. Additionally, some minor failures (such as gain drift and nonzero offset) of phase current sensors would lead to torque pulsation synchronizing with the inverter output frequency [1]. The larger offset and scaling error of phase current sensors would bring about the worse performance of torque regulation. Moreover, if the offset and gain drift are above some certain level, it would cause over-current trip under high speed and heavy load conditions [2]. So it is necessary to consider fault tolerant operation of phase current sensor failure.

The current sensorless technology, regarded as fault tolerant one, has been developed in the past few decades. Its core lies in that the physical fault current sensor is replaced with virtual sensor (or current estimator). This technology has several advantages such as high reliability and low cost as well as space and weight savings owing to omitting physical current sensor. Moreover, it allows the drive system to work in hostile environment.

As far as the current sensorless technique is concerned, three estimation solutions have been reported in the literature. The first one is a DC-link current-based approach which restructures phase currents with the information of the DC-link current and switching states in VSI [3]. Although it is mainstream method, its unavoidable drawbacks are exposed: the duration of an active switching state may be so short that the DC-link current cannot be measured on one hand, on the other hand, there are immeasurable regions in the output voltage hexagon where the DC-link current sampling and reconstruction are limited or impossible to do [4]. In addition, the DC-link sensed current remains sensitive to the narrow pulse and further deteriorates if the cable capacitance causes spurious oscillations in the DC-link waveform. In order to provide high-accuracy phase current reconstruction over a wide range of operating conditions with a low current waveform, over the past years, many kinds of methods of improved PWM modulation strategy have been proposed for the single DC-link current sensor technique [5]-[14]. Although many improvement methods show reasonable phase current reconstruction performance, these methods suffer from complicated algorithms [15]. The second one is an analytical model-based approach. In [16], on the base of the voltage and flux equations of induction motor (IM) drive, the phase current is estimated by using the synchronous reference

frame variables under single phase current sensor condition. In [17], by the discrete voltage equations of PMSM drive, the phase currents are estimated. Although it is easier to implement than the first one, the method isn't robust against the variation of system parameters. The third one is an adaptive observer-based approach. In [18], the phase current is reconfigured for IM drive using single phase current sensor, while in [19], the phase currents are reconfigured for PMSM drive without any phase current sensors. Compared with the first two solutions, the third solution has stronger robust against the variation of system parameters [20]-[21]. For PMSM drive system when only one phase current sensor is available, the remaining two phase currents estimation based on an adaptive observer must be studied, which is required to perform current feedback control. However, there is no literature on such strategy.

For PMSM drive system, model predictive torque control (MPTC) is an emerging control strategy [22]-[29]. Its main objective is to control instantaneous torque and stator flux with high accuracy and thus MPTC plays an important role to ensure the quality of the torque and speed control. MPTC adopts the principle of model predictive control (MPC) and can provide high dynamic performance and low stator current harmonic.

For conventional PI-based MPTC PMSM drive system, its speed regulator employs the algorithm of PI. In general, PI may perform well under certain operating condition, but it doesn't work properly and thus degrades dynamic performance under other operating conditions such as variation of system parameters and external disturbances. To improve the robustness of the speed regulator, some techniques have been proposed in recent years [30]-[34]. Except these techniques, a global fast terminal sliding mode (GFTSM) control is an effective and practical one [35]-[36], which is based on sliding mode theory and employs the fast terminal sliding mode in both the reaching stage and sliding stage. By adding the nonlinear function to the sliding mode surface, the GFTSM controller can enable drive system not only to be superior robust against system uncertainties and external disturbances but also to have quick response as well as high control precision. Even so, studies on GFTSM speed regulator are very few. In this paper, we propose replacement of PI with GFTSM for MPTC PMSM drive system.

In this paper, by referring to the adaptive approach and integrating the GFTSM method, a new GFTSM-based MPTC strategy with the adaptive observer is put forward for the PMSM drive system with single phase current sensor. The proposed adaptive observer presents a satisfactory the remaining two phase currents tracking performance in the presence of stator resistance change caused by the temperature variation. And the designed the GFTSM controller enhances the speed regulator's robustness against parameter uncertainty and external disturbance. On the basis of the above foundation, the synthesized MPTC PMSM drive control system achieves a high performance.

This paper is organized as follows: Dynamic model of PMSM drive is presented in Section II. Section III gives the adaptive observer and GFTSM speed regulator design as well as MPTC design. Experimental results and analysis are presented in Section IV. Section V contains the conclusions.

Notation: The following nation is used throughout this paper. $\bullet_{\mathrm{d}}$, $\bullet_{\mathrm{q}}$, $\bullet_{\alpha}$ and $\bullet_{\beta}$ are used to denote the d axis, q axis, α axis and β axis component of $\bullet$, respectively; $\bullet^{*}$ is used to denote the reference values of $\bullet$; $\hat{\bullet}$ is used to denote the estimate of $\bullet$; $\tilde{\bullet}$ is used to denote the parameter estimation error of $\bullet$; $\bullet^{k}$ and $\bullet^{k+1}$ are used to denote the instant value at kth and $(k+1)$th of $\bullet$, respectively.

II. Dynamic Model of PMSM Drive

As for three-phase PMSM drive, the models in rotor synchronous reference frame (dq-frame) and two-phase stationary reference frame ($\alpha\beta$-frame) are expressed as follows, respectively,

$$\begin{cases} \dfrac{\mathrm{d}i_d}{\mathrm{d}t} = \dfrac{1}{L_d}(u_d - R_s i_d + \mathrm{p}\omega_r L_q i_q) \\ \dfrac{\mathrm{d}i_q}{\mathrm{d}t} = \dfrac{1}{L_q}(u_q - R_s i_q - \mathrm{p}\omega_r (L_d i_d + \psi_m)) \end{cases} \tag{1}$$

$$\begin{cases} \dfrac{\mathrm{d}i_\alpha}{\mathrm{d}t} = \dfrac{1}{L_\alpha}(u_\alpha - R_s i_\alpha + \mathrm{p}\omega_r \psi_m \sin\theta) \\ \dfrac{\mathrm{d}i_\beta}{\mathrm{d}t} = \dfrac{1}{L_\beta}(u_\beta - R_s i_\beta - \mathrm{p}\omega_r \psi_m \cos\theta) \end{cases} \tag{2}$$

And the mechanical equation is expressed as

$$\frac{\mathrm{d}\omega_r}{\mathrm{d}t} = \frac{1}{J}\left(T_e - T_l - B\omega_r - T_f\right) \tag{3}$$

where the electromagnetic torque T_e is expressed as

$$T_e = \frac{3\mathrm{p}}{2}\left[\psi_m i_q + \left(L_d - L_q\right) i_d i_q\right] \tag{4}$$

III. Design of GFTSM-based MPTC PMSM drive System with Adaptive Observer

The objective of GFTSM-based MPTC using adaptive observer is that the PMSM drive system can work reliably and its speed and torque can be controlled not only to have satisfactory performance but also to be strong robust to parameters variation and external disturbance. The schematic of the proposed control system is shown in Fig.1.Our design task concentrates on adaptive observer, GFTSM speed regulator and MPTC as follows.

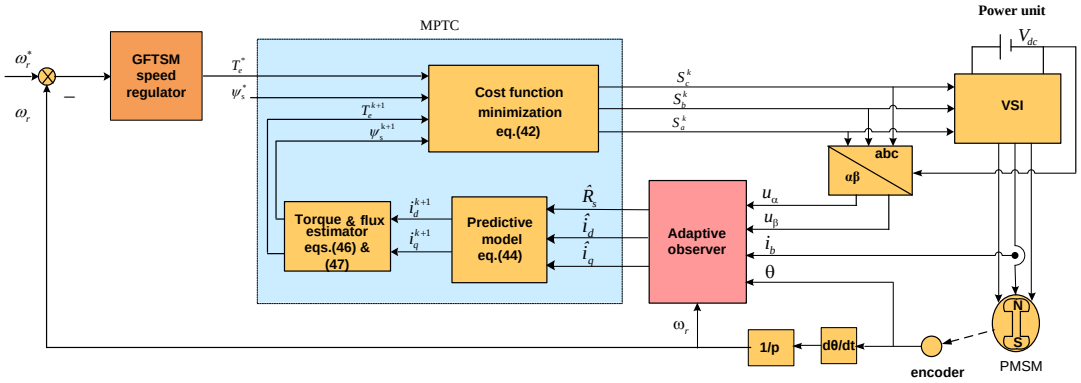

Fig. 1 Block diagram of GFTSM-based MPTC PMSM drive system with adaptive observer

A. *Adaptive observer design*

The proposed adaptive observer is to estimate the remaining two phase currents and stator resistance when single phase current sensor is available. In the design process, assume the following conditions.

(1) Only phase-*b* current can be measured and the remaining two phase current sensors are not available.

(2) Due to heating during operating of the motor, the stator resistance R_s is considered as a time-varying parameter.

(3) There is no saturation in the magnetic circuit.

For surface-mounted PMSM drive, $L_d=L_q=L_\alpha=L_\beta=L$. The α-axis in $\alpha\beta$-frame is oriented along phase-*a* axis in three-phase stationary reference frame (*abc*-frame). The *abc*-axes stator currents in *abc*-frame can be obtained from the $\alpha\beta$-axes ones in $\alpha\beta$-frame by the following transformation matrix,

$$\begin{bmatrix} i_a \\ i_b \\ i_c \end{bmatrix} = \begin{bmatrix} 1 & 0 \\ -1/2 & \sqrt{3}/2 \\ -1/2 & -\sqrt{3}/2 \end{bmatrix} \begin{bmatrix} i_\alpha \\ i_\beta \end{bmatrix} \tag{5}$$

where i_a, i_b and i_c are *abc*-axes stator currents in *abc*-frame. From (5), the following equation can be given,

$$i_b = -\frac{1}{2} i_\alpha + \frac{\sqrt{3}}{2} i_\beta \tag{6}$$

Taking (2) into account, the time derivative of (6) is deduced as follows:

$$\begin{aligned} \frac{\mathrm{d}i_b}{\mathrm{d}t} &= \frac{\sqrt{3}}{2L}[u_\beta - R_s(\frac{1}{\sqrt{3}} i_\alpha + \frac{2}{\sqrt{3}} i_b) - \mathrm{p}\omega_r \psi_\mathrm{m} \cos\theta] - \\ &\quad \frac{1}{2L}(u_\alpha - R_s i_\alpha + \mathrm{p}\omega_r \psi_\mathrm{m} \sin\theta) \\ &= \frac{\sqrt{3}u_\beta - u_\alpha - 2R_s i_b - \mathrm{p}\omega_r \psi_\mathrm{m}(\sqrt{3}\cos\theta + \sin\theta)}{2L} \end{aligned} \tag{7}$$

The following adaptive observer is proposed in order to estimate phase-*b* current,

$$\begin{aligned} \frac{\mathrm{d}\hat{i}_b}{\mathrm{d}t} &= \frac{\sqrt{3}}{2L}[u_\beta - \hat{R}_s(\frac{1}{\sqrt{3}} \hat{i}_\alpha + \frac{2}{\sqrt{3}} i_b) - \mathrm{p}\omega_r \psi_\mathrm{m} \cos\theta] - \\ &\quad \frac{1}{2L}(u_\alpha - \hat{R}_s \hat{i}_\alpha + \mathrm{p}\omega_r \psi_\mathrm{m} \sin\theta) - k_1 f(\tilde{i}_b) - k_2 \tilde{i}_b \\ &= \frac{1}{2L}[\sqrt{3}u_\beta - u_\alpha - 2\hat{R}_s i_b - \mathrm{p}\omega_r \psi_\mathrm{m}(\sqrt{3}\cos\theta + \\ &\quad \sin\theta)] - k_1 f(\tilde{i}_b) - k_2 \tilde{i}_b \end{aligned} \tag{8}$$

where $k_1 f(\tilde{i}_b)$ and $k_2 \tilde{i}_b$ are correctors, k_1 and k_2 are the positive observer gains, and $f(.)$ denotes the nonlinear function of phase-*b* current estimation error $\tilde{i}_b$, which is defined as,

$$\tilde{i}_b = \hat{i}_b - i_b \tag{9}$$

Definite the following stator resistance estimation error,

$$\tilde{R}_s = \hat{R}_s - R_s \tag{10}$$

By subtracting (8) from (7), the dynamics equation of the phase-*b* current estimation error is given as follows:

$$\frac{\mathrm{d}\tilde{i}_b}{\mathrm{d}t} = -\frac{1}{L}\tilde{R}_s i_b - k_1 f(\tilde{i}_b) - k_2 \tilde{i}_b \tag{11}$$

In order to determine the adaptive law of the stator resistance and the observer gains, construct the candidate Lyapunov function as

$$V_1 = \frac{1}{2}(\tilde{i}_b^2 + \frac{1}{r}\tilde{R}_s^2) \tag{12}$$

where r is constant positive scalar.

The time derivative of (12) is obtained as follows,

$$\frac{\mathrm{d}V_1}{\mathrm{d}t} = -k_2 \tilde{i}_b^2 - k_1 f(\tilde{i}_b)\tilde{i}_b + \tilde{R}_s(\frac{1}{r}\frac{d\tilde{R}_s}{dt} - \frac{1}{L} i_b \tilde{i}_b) \tag{13}$$

If we define following equality,

$$\frac{1}{r}\frac{\mathrm{d}\tilde{R}_s}{\mathrm{d}t} - \frac{1}{L} i_b \tilde{i}_b = 0 \tag{14}$$

(13) can be rewritten as below

$$\frac{\mathrm{d}V_1}{\mathrm{d}t} = -k_2 \tilde{i}_b^2 - k_1 f(\tilde{i}_b)\tilde{i}_b \tag{15}$$

To render $\dot{V}_1$ negative, we assume

$$f(\tilde{i}_b) = \mathrm{sign}(\tilde{i}_b) \tag{16}$$

As a result, the following inequality is satisfied

$$\frac{\mathrm{d}V_1}{\mathrm{d}t} < 0$$

By Lyapunov stability theorem, dynamics system (11) is stable, which means that both $\tilde{i}_b$ and $\tilde{R}_s$ can converge to zero. Since the variation of the stator resistance in the observer time scale is negligible, i.e.,

$$\frac{\mathrm{d}R_s}{\mathrm{d}t} \approx 0$$

then the following formula holds

$$\frac{\mathrm{d}\tilde{R}_s}{\mathrm{d}t} = \frac{\mathrm{d}\hat{R}_s}{\mathrm{d}t} - \frac{\mathrm{d}R_s}{\mathrm{d}t} \approx \frac{\mathrm{d}\hat{R}_s}{\mathrm{d}t} \tag{17}$$

Therefore, from (14), the adaptive mechanism of the stator resistance is derived as follows:

$$\hat{R}_s = \frac{r}{L}\int (i_b \tilde{i}_b)\mathrm{d}t \tag{18}$$

With the adaptive mechanism in (18), the estimation value of the stator resistance can converge to its real value.

In order to improve the estimation accuracy of the stator resistance and to ensure a null steady error, on the base of PI strategy, (18) is modified as below,

$$\hat{R}_s = \frac{r}{L}\{K_{P(R_s)}[i_b(\hat{i}_b - i_b)] + K_{I(R_s)}\int[i_b(\hat{i}_b - i_b)]\mathrm{d}t\} \qquad (19)$$

where $K_{P(R_s)}$ and $K_{I(R_s)}$ are proportional and integral scalars, respectively.

By replacing R_s in (2) with $\hat{R}_s$ in (19), the $\alpha\beta$-axes currents observer can be constructed as follows,

$$\begin{cases} \dfrac{\mathrm{d}\hat{i}_\alpha}{\mathrm{d}t} = \dfrac{1}{L}(u_\alpha - \hat{R}_s\hat{i}_\alpha + \mathrm{p}\omega_r\psi_\mathrm{m}\sin\theta) \\ \dfrac{\mathrm{d}\hat{i}_\beta}{\mathrm{d}t} = \dfrac{1}{L}(u_\beta - \hat{R}_s\hat{i}_\beta - \mathrm{p}\omega_r\psi_\mathrm{m}\cos\theta) \end{cases} \qquad (20)$$

By combining (8), (19) and (20), the block diagram of the designed adaptive observer is established as shown in Fig. 2, which treats the stator voltages, rotor electrical position and speed as the inputs, the *dq*-axes currents and stator resistance as outputs when only phase-*b* current is measured.

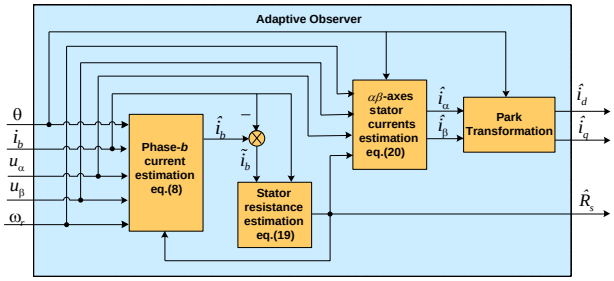

Fig. 2 Block diagram of the proposed adaptive observer

Remark 1. From Fig. 2, it can be seen that estimating the phase-*b* current is a key step and primary premise in construction of the adaptive observer. The error between the phase-*b* measured current and its estimated value must be guaranteed to converge towards zero.

Remark 2. From (8) and (19), it can be seen that although the coupling relationship between $\hat{i}_b$ and $\hat{R}_s$ exists, the design process does not need to calculate decouple of them. In fact, the phase-*b* current estimation equation (8) and the stator resistance adaptive law (19) are implemented and solved all together.

Remark 3. The convergence rate of the observer is dependent on the observer gains k_1 and k_2, which should be chosen to be large enough such that the observer responds as soon as possible.

Remark 4. The estimated *dq*-axes currents in Fig.2 will be applied to MPTC as shown in Fig.1.

Remark 5. From (5), the estimation of phase-*a* current in *abc*-frame is equal to that of α-axis current in $\alpha\beta$-frame as follows,

$$\hat{i}_a = \hat{i}_\alpha \qquad (21)$$

Accordingly, the estimation of phase-*c* current in *abc*-frame can be obtained as follows,

$$\hat{i}_c = -\left(i_b + \hat{i}_\alpha\right)$$

Remark 6. The proposed adaptive observer is robust against only the stator resistance change. If other parameter certainties (such as stator inductance change and permanent magnet flux change, etc.) and unmodeled dynamics are required to be considered, then adaptive robust method with extended state observer can be borrowed from [20] and [33], which is our next research topic.

B. GFTSM speed regulator design

1) GFTSM design

Define the speed error as,

$$e = \omega_r^* - \omega_r$$

Let

$$x_1 = e, x_2 = \dot{x}_1,\ u = \dot{T}_e \qquad (22)$$

Assume that ω_r^* (or $\dot{\omega}_r^*$), T_l, T_f are constant and ω_r has continuous second-order derivative. Then the state equation of (3) can be expressed as following

$$\begin{cases} \dot{x}_1 = x_2 \\ \dot{x}_2 = -\dfrac{B}{J}x_2 - \dfrac{1}{J}u \end{cases} \qquad (23)$$

where u can be regarded as the control input.

Our target is to enable the drive system to be strong robust and to have very fast response. For this reason, based on sliding mode theory, GFTSM speed regulator is employed. Fast terminal sliding mode surface is designed as following,

$$s = \dot{x}_1 + \alpha x_1 + \beta x_1^{q/p} \qquad (24)$$

where $\alpha, \beta > 0, q, p(q < p)$ are positive odd integers.

Taking the first-order derivative of (24) yields

$$\dot{s} = \left(\alpha - \frac{B}{J}\right)x_2 - \frac{1}{J}u + \beta\frac{\mathrm{d}}{\mathrm{d}t}\left(x_1^{q/p}\right) \qquad (25)$$

To make the system (23) reach the sliding mode surface in finite time, the fast terminal attractor is adopted as follows,

$$\dot{s} = -\varphi s - \gamma s^{v/m} \qquad (26)$$

Where $\varphi > 0, \gamma > 0, m > v > 0$, m and v are odd integers.

Let (25) be equal to (26) and thus the following sliding mode control law can be obtained

$$u = J\left(\left(\alpha - \frac{B}{J}\right)x_2 + \beta\frac{\mathrm{d}}{\mathrm{d}t}\left(x_1^{q/p}\right) + \varphi s + \gamma s^{v/m}\right) \qquad (27)$$

By combining (23), (24) and (27), the block diagram of the designed GFTSM speed regulator is shown as in Fig. 3.

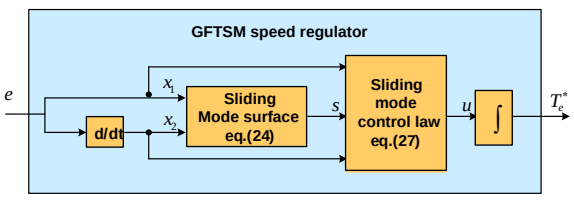

Fig. 3 Block diagram of the designed GFTSM speed regulator

By solving differential equation (26), the time from any state $s(0) \neq 0$ to the sliding mode surface $s(t_f) = 0$ can be derived as follows

$$t_f = \frac{m}{\varphi(m\text{-}v)} \ln \frac{\varphi(s(0))^{(m-v)/m} + \gamma}{\gamma} \tag{28}$$

Remark 1. From (27), it can be seen that the sliding mode control law doesn't include switching item and thus weakens system chatter.

Remark 2. Under control law (27), one can easily see that if *s* converges to zero according to the terminal attractor (26), x_1 will accordingly converges to zero in terms of the following fast terminal attractor

$$\dot{x}_1 = -\alpha x_1 - \beta x_1^{q/p} \tag{29}$$

It can be observed from (26) and (29) that the fast terminal attractors are adopted both in the reaching phase and in sliding phase. Consequently, the designed regulator (27) is a global terminal sliding mode one which guarantees the finite time control performance.

Remark 3. According to (28), t_f can be set arbitrarily by adjusting parameters of m,v, φ, γ.

Remark 4. The designed GFTSM speed regulator (27) is not only stable but also robust, which will be analyzed as below.

2) Stability analysis

Construct Lyapunov function as

$$V_2 = s^2/2 \tag{30}$$

Differentiating (30) yields

$$\dot{V}_2 = s\dot{s} = -\varphi s^2 - \gamma s^{(m+v)/m}$$

Since $(m+v)$ is even, therefore $\dot{V} = s\dot{s} < 0$. According to Lyapunov stability theory, the system (23) is stable and its movement can tend to sliding mode surface and finally reach the sliding mode.

3) Robustness analysis

Considering parameter uncertainties and external disturbances, the system (23) are rewritten as following

$$\begin{cases} \dot{x}_1 = x_2 \\ \dot{x}_2 = -\dfrac{B}{J} x_2 - \dfrac{1}{J} u + d(x_1, x_2) \end{cases} \tag{31}$$

where $d(x_1, x_2)$ can be regarded as the total disturbance including uncertainties and external disturbances. Assume $|d(x_1, x_2)| \leq L$, L is maximum value.

As for system (31), differentiating (24) yields

$$\dot{s} = \left(\alpha - \frac{B}{J}\right) x_2 - \frac{1}{J} u + d(x_1, x_2) + \beta \frac{\mathrm{d}}{\mathrm{d}t}\left(x_1^{q/p}\right) \tag{32}$$

Substituting (27) into (32) yields

$$\begin{aligned} \dot{s} &= -\varphi s - \gamma s^{v/m} + d(x_1, x_2) \\ &= -\varphi s - \left(\gamma - \frac{d(x_1, x_2)}{s^{v/m}}\right) s^{v/m} \end{aligned} \tag{33}$$

Let

$$\bar{\gamma} = \gamma - \frac{d(x_1, x_2)}{s^{v/m}} \tag{34}$$

Then (33) can be rewritten as

$$\dot{s} = -\varphi s - \bar{\gamma} s^{v/m} \tag{35}$$

To make (35) be a fast terminal attractor, (34) must satisfy $\bar{\gamma} > 0$. Therefore, the following inequality holds true

$$\gamma - \frac{d(x_1, x_2)}{s^{v/m}} > \gamma - \frac{\left|d(x_1, x_2)\right|}{\left|s^{v/m}\right|} > \gamma - \frac{L}{\left|s^{v/m}\right|} > 0$$

Then we can deduce

$$\gamma > \frac{L}{\left|s^{v/m}\right|} \tag{36}$$

(36) is equivalent to

$$|s| > \left(\frac{L}{\gamma}\right)^{\mathrm{m/v}} \tag{37}$$

As a result, the fast terminal convergence region Δ is constrained by

$$\Delta = \left\{ x_1, x_2 : |s| \leq \left(\frac{L}{\gamma}\right)^{\mathrm{m/v}} \right\} \tag{38}$$

Furthermore, we assume

$$\gamma = \frac{L}{\left|s^{v/m}\right|} + \eta, \eta > 0 \tag{39}$$

According to (35), the time from any state $s(0) \neq 0$ to the sliding surface is deduced as follows

$$\bar{t}_f = \frac{\mathrm{m}}{\varphi(\mathrm{m\text{-}v})} \ln \frac{\varphi(s(0))^{(\mathrm{m-v})/\mathrm{m}} + \bar{\gamma}}{\bar{\gamma}} \tag{40}$$

Since $\bar{\gamma} > \eta$ the following inequality can be deduced

$$\ln \frac{\varphi(s(0))^{(\mathrm{m-v})/\mathrm{m}} + \bar{\gamma}}{\bar{\gamma}} \leq \ln \frac{\varphi(s(0))^{(\mathrm{m-v})/\mathrm{m}} + \eta}{\eta}$$

And then the reaching time satisfies

$$\bar{t}_f \leq \frac{\mathrm{m}}{\varphi(\mathrm{m\text{-}v})} \ln \frac{\varphi(s(0))^{(\mathrm{m-v})/\mathrm{m}} + \eta}{\eta} \tag{41}$$

Through the above analysis, it can be seen that if the condition $\bar{\gamma} > 0$ holds hence fast terminal convergence can be guaranteed and system (31) can reach neighborhood Δ of the sliding mode surface $s(\bar{t}_f) = 0$ in finite time $\bar{t}_f$.

C. Model predictive torque control

The basic idea of MPTC is to predict the future behavior of the variables over a time frame based on the model of the system. As shown in Fig.1, MPTC includes three parts: cost function minimization, predictive model and flux & torque estimator.

1) Cost function minimization

For MPTC, the cost function is such chosen that both torque and flux at the end of the cycle is as close as possible to the reference value. Generally, the minimum value of cost function is defined as

$$\begin{aligned} &\min.g = \left|T_e^* - T_e^{k+1}\right| + k_3\left\|\psi_s^*\right| - \left|\psi_s^{k+1}\right\| \\ &s.t.\quad u_s^k \in \{V_1,\ V_2,\ \cdots\ V_5,\ V_6\} \end{aligned} \tag{42}$$

where V_1, V_2, V_3, V_4, V_5, and V_6 are six nonzero voltage space vectors and can be generated by three phase VSI with respect to the different switches states. A set of voltage space vectors u_s^k at kth instant is defined as

$$u_s^k = 2V_{dc}\left[S_a^k + e^{i2\pi/3}S_b^k + \left(e^{i2\pi/3}\right)^2 S_c^k\right]/3 \tag{43}$$

where S_x^k (x=a,b,c) at kth instant is upper power switch state of one of three legs . S_x^k =1 or S_x^k =0 when upper power switch of one leg is on or off. k_3 is the weighting factor.

In order to compensate inherent one-step delay which exists in practical digital system, the cost function (42) is revised as below

$$\begin{aligned} &\min.g = \left|T_e^* - T_e^{k+2}\right| + k_3\left\|\psi_s^*\right| - \left|\psi_s^{k+2}\right\| \\ &s.t.\quad u_s^k \in \{V_1,\ V_2,\ \cdots\ V_5,\ V_6\} \end{aligned} \tag{44}$$

2) Predictive model for stator currents

According to (1), the prediction of the stator current at the next sampling instant is expressed as

$$\begin{cases} i_d^{k+1} = i_d^k + \dfrac{1}{L}(-R_s i_d^k + \mathrm{p}\omega_r^k L i_q^k + u_d^k)T_s \\ i_q^{k+1} = i_q^k + \dfrac{1}{L}(-R_s i_q^k - \mathrm{p}\omega_r^k L i_d^k - \mathrm{p}\omega_r^k \psi_m + u_q^k)T_s \end{cases} \tag{45}$$

where i_d^k , i_q^k and R_s are replaced by the corresponding estimated values coming from the observer in Fig.2. T_s is the sampling period.

3) Torque & flux estimators

In dq-frame, the current-based flux-linkage ψ_d and ψ_q can be expressed as following vector,

$$\begin{bmatrix} \psi_d^{k+1} \\ \psi_q^{k+1} \end{bmatrix} = \begin{bmatrix} L & 0 \\ 0 & L \end{bmatrix}\begin{bmatrix} i_d^{k+1} \\ i_q^{k+1} \end{bmatrix} + \begin{bmatrix} \psi_m \\ 0 \end{bmatrix} \tag{46}$$

The magnitude of stator flux linkage ψ_s is

$$\psi_s^{k+1} = \sqrt{\left(\psi_d^{k+1}\right)^2 + \left(\psi_q^{k+1}\right)^2} \tag{47}$$

Electromagnetic torque developed in dq- frame can be estimated as following

$$T_e^{k+1} = \frac{3}{2}\mathrm{p}\psi_m i_q^{k+1} \tag{48}$$

Substituting (45) into (48), the torque can be calculated.

IV. Simulation Result and Analysis

In order to validate the effective of proposed control strategy, the designed control system as shown in Fig.1 has been implemented in Matlab/Simulink/Simscape platform. The parameters of PMSM are given in Table 1. The sampling period is 100 μ s, and value k_3 is selected to be 200. The reference stator flux ψ_s^* is 0.175Wb. The parameters of the adaptive observer are

$$K_{P(R_s)} = 0.006, K_{I(R_s)} = 8, k_1 = 30, k_2 = 5000, r = 1000$$

The parameters of GFTSM in Fig.3 are determined as follows,

$$\alpha = 100, \beta = 250, p = 7, q = 5, \varphi = 1000, \gamma = 80000, m = 3, v = 1$$

TABLE1 Parameters of PMSM

Symbol	Value	Symbol	Value
R_s	2.875Ω	ω_r^*	1000rpm
L_d , L_q	0.0085H	T_n	4N.m
ψ_m	0.175Wb	J	0.0008Kg.m^2
p	4	B_m	0.001Nms
V_{dc}	300V	T_f	0

A. The GFTSM-based MPTC PMSM drive system comparison between the one with single phase current sensor and the other with two phase current sensors

In order to verify estimation accuracy of the observer for GFTSM-based MPTC PMSM drive system with single phase current sensor, two scenarios of numerical simulation are provided and compared, which correspond to PMSM system with two phase current sensors (phase-*a* and -*b* sensors) and PMSM system with single phase current sensor (phase-*b*), respectively. For convenience sake, the former scenario is marked as Case one and the latter one as Case two. Except the above-mentioned different number of current sensor, two systems employ completely identical the GFTSM-based MPTC strategy.

Fig.4 shows comparison of two scenarios in terms of stator currents, stator resistance, rotor speed and torque when the reference speed n^* is set to 1000 rpm, the load torque is increased from 0 N.m to 4 N.m at 0.1 seconds and the stator resistance is changed from its nominal value 2.875 Ω to 5 Ω at 0.3 seconds.

From Fig.4(a)-4(c), it can be seen that, for designed adaptive observer of Case two, its estimated *a*-axis and *c*-axis currents in *abc*-frame rapidly track corresponding ones of Case one, and its estimated stator resistance can rapidly follow actual resistance change and converge to its actual value accurately. Fig. 4(d)-4(e) show that, for GFTSM-based MPTC system of Case two, its speed and torque can be regulated in a satisfactory manner and it has almost as good performance as GFTSM-based MPTC system of Case one.

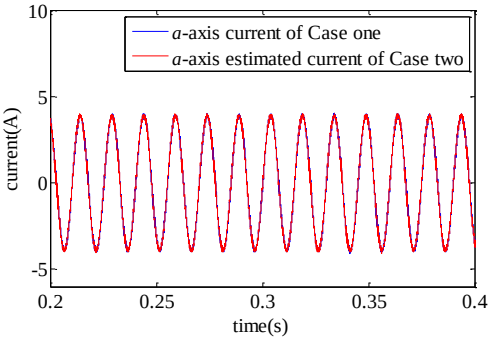

(a) *a*-axis stator current in *abc*-frame

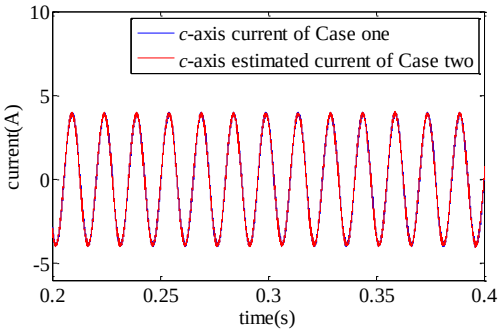

(b) *c*-axis stator current in *abc*-frame

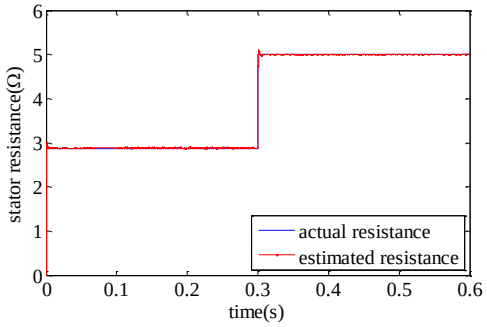

(c) Actual and estimated stator resistance

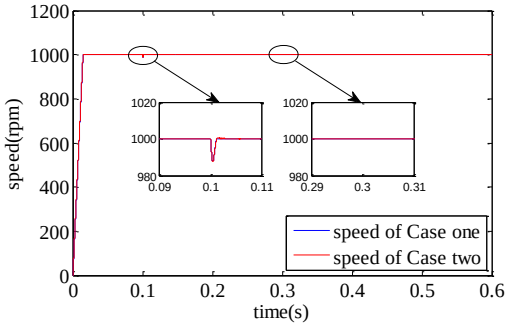

(d) Rotor speed response

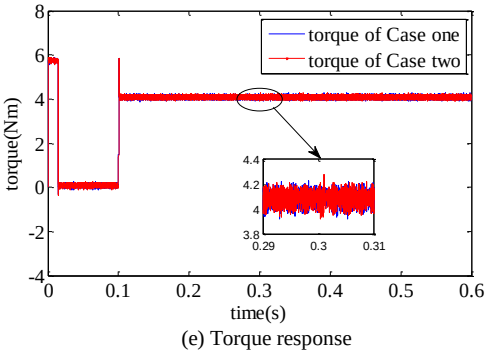

(e) Torque response

Fig.4 Dynamic response comparison between Case one and Case two under the variation of stator resistance

B. The MPTC PMSM system comparison between the one based on PI and the other based on GFTSM

For GFTSM-based MPTC PMSM systems, for the sake of verifying its stronger robustness, two systems are compared, which correspond to the PI-based and GFTSM-based MPTC PMSM systems, respectively. Except distinct outer-loop speed regulator (i.e. PI and GFTSM), two systems employ completely identical MPTC and adaptive observer. In the simulation, their reference speeds $n^*$are set to 1000 rpm, their load torques of 0 N.m are increased to 4 N.m at 0.1 seconds and stator resistance is its nominal value 2.875 Ω .

In the simulation, sampling values of three-phase currents are recorded over the time range from 0.1 seconds to 0.2 seconds. During this period, the fundamental frequency of three-phase currents is 66.67 Hz. Total harmonic distortion (THD) can be obtained by comparing the higher frequency components to the fundamental one.

1) The comparison of anti-load variation ability under the same speed transient response

The parameters of PI for PI-based MPTC PMSM system are adjusted as follows,

$$K_P = 0.7, K_I = 0.03$$

such that PI-based MPTC system has almost the same speed transient response as GFTSM-based one.

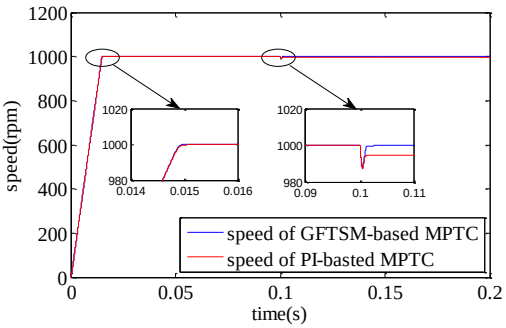

(a) Rotor speed response

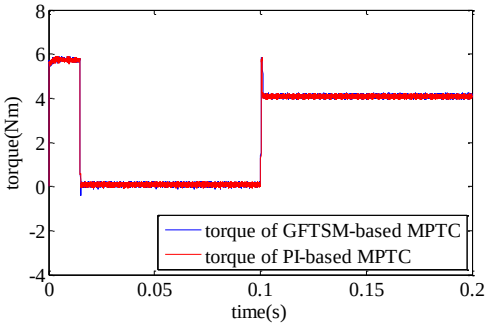

(b) Torque response

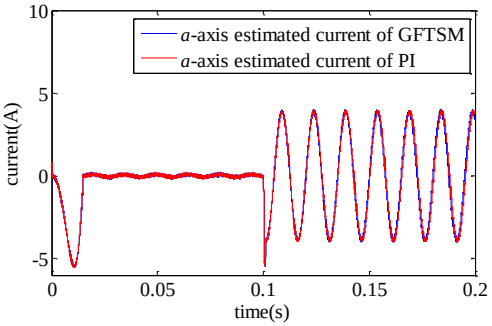

(c) *a*-axis stator current in *abc*-frame

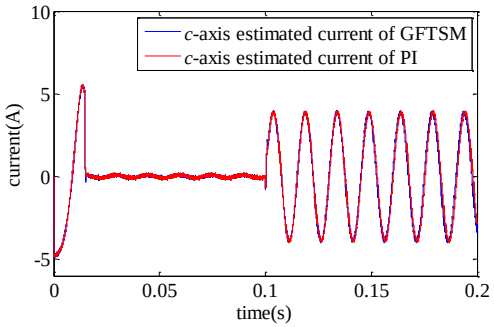

(d) *c*-axis stator current in *abc*-frame

Fig.5 The comparison of anti-load variation ability under the same speed transient response

TABLE 2 THD of Three-phase Stator Currents

Control scheme	i_a	i_b	i_c
PI-based MPTC	2.21%	2.32%	2.24%
GFTSM-based MPTC	1.84%	1.88%	1.85%

Figs.5 shows their dynamical responses in terms of speed, torque and stator currents. Fig.5(a) intuitively gives their speed response comparison, which demonstrates that for GFTSM-based MPTC PMSM system, its speed can sharply adapt to the change of external load in a satisfactory manner, and its capable of accommodating the challenge of load disturbance is superior to PI-based one's. From Fig.5(b)-5(d), it can be observed that for two systems with same adaptive observer, their torques, estimated *a*-axis and *c*-axis currents in *abc*-frame are almost the same.

Table 2 shows THD comparison of three-phase currents. From Table 2, what can be observed is that the THD of the GFTSM-based MPTC is smaller than one of the PI-based MPTC.

2) The comparison of dynamic responses under the same anti-load variation ability

The parameters of PI for PI-based MPTC PMSM system are adjusted as follows,

$$K_P = 3, K_I = 0.1$$

such that PI-based MPTC system has almost the same anti-load variation ability as GFTSM-based one.

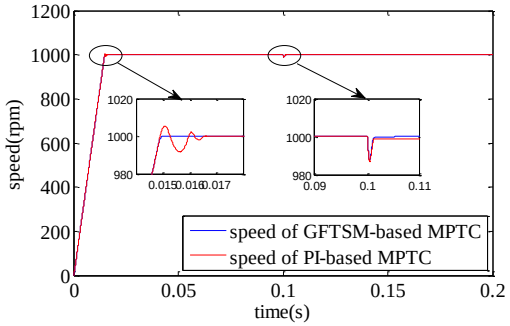

(a) Rotor speed response

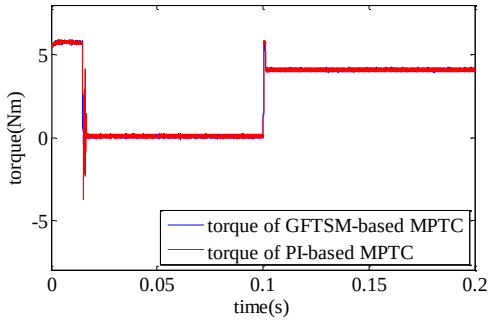

(b) Torque response

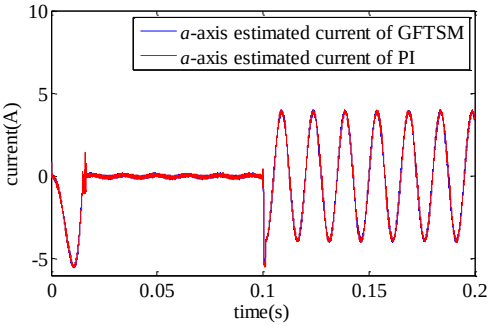

(c) *a*-axis stator current in *abc*-frame

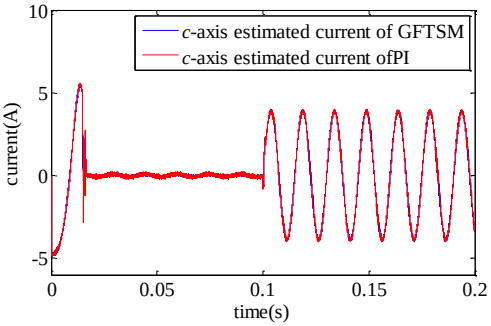

(d) *c*-axis stator current in *abc*-frame

Fig.6 The comparison of dynamic responses under the same anti-load variation ability

Figs.6(a)-6(d) show their dynamical responses in terms of speed, torque and stator currents. Fig. 6(a) intuitively gives their speed response comparison, which indicates that GFTSM-based MPTC PMSM system has smaller overshoot and faster settling time than PI-based one. Meanwhile, it can be found from Fig.6(b) that the torque response of GFTSM-based MPTC PMSM system is better than one of PI-based one. From Fig.6(c)-6(d), it can be observed that, their estimated *a*-axis and *c*-axis currents in *abc*-frame are almost the same.

C. The MPTC PMSM system comparison between the one based on SM and the other based on GFTSM

Here, the working condition of PMSM drive system is identical with Section B.

For SM-based speed regulator, its sliding mode surface and its reaching law are selected as following,

$$s = ce + \dot{e} \tag{49}$$

$$\dot{s} = -k_4 s - \varepsilon \operatorname{sign}(s) \tag{50}$$

1) The comparison of anti-load variation ability under the

same speed transient response

The parameters of SM for SM-based MPTC PMSM system are adjusted as follows,

$$c = 160,\ k_4 = 800,\ \ \varepsilon = 3\times 10^5$$

such that SM-based MPTC system has almost the same speed transient response as GFTSM-based one.

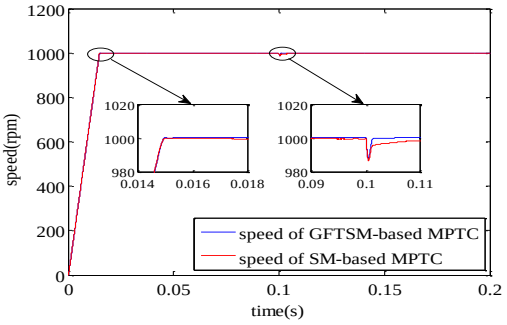

(a) Rotor speed response

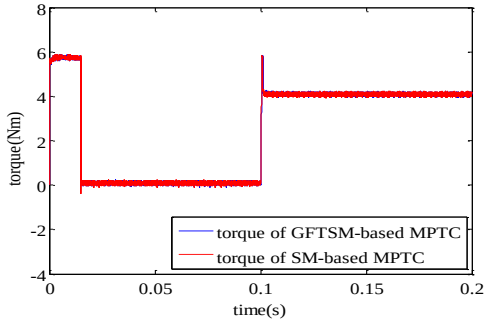

(b) Torque response

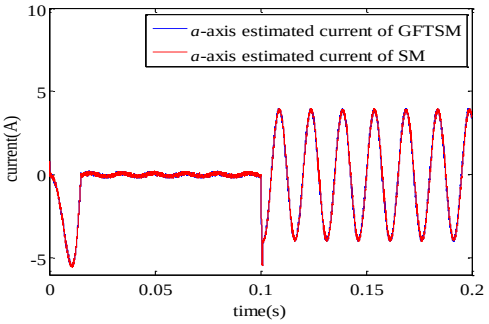

(c) *a*-axis stator current in *abc*-frame

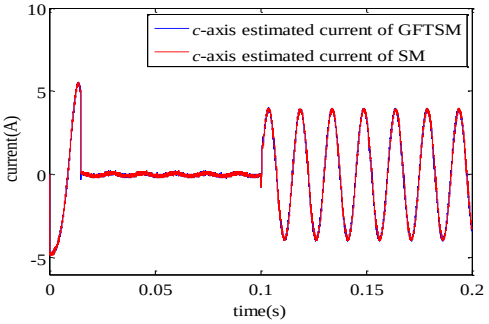

(d) *c*-axis stator current in *abc*-frame

Fig.7 The comparison of anti-load variation ability under the same speed transient response

TABLE 3 THD of Three-phase Stator Currents

Control scheme	i_a	i_b	i_c
SM-based MPTC	2.01%	2.12%	2.14%
GFTSM-based MPTC	1.84%	1.88%	1.85%

Figs.7(a)-7(d) show their dynamical responses in terms of speed, torque and stator currents. Fig.7(a) illustrates that for GFTSM-based MPTC PMSM system, benefiting from the fast terminal sliding mode employed in both the reaching stage and the sliding stage, its recovery rate of speed response is obviously faster than SM-based one's. From Figs.7(b)-7(d), it can be seen that for two systems with same adaptive observer, their torques, estimated *a*-axis and *c*-axis currents in *abc*-frame are almost the same.

Table 3 shows THD comparison of three-phase currents. From Table 3, what can be observed is that the THD of the GFTSM-based MPTC is smaller than one of the SM-based MPTC.

2) The comparison of dynamic responses under the same anti-load variation ability

The parameters of SM for SM-based MPTC PMSM system are adjusted as follows,

$$c = 140,\ k_4 = 2500,\ \ \varepsilon = 3\times 10^7$$

such that SM-based MPTC system has almost the same anti-load variation ability as GFTSM-based one.

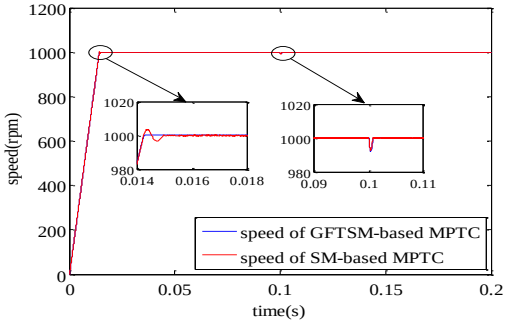

(a) Rotor speed response

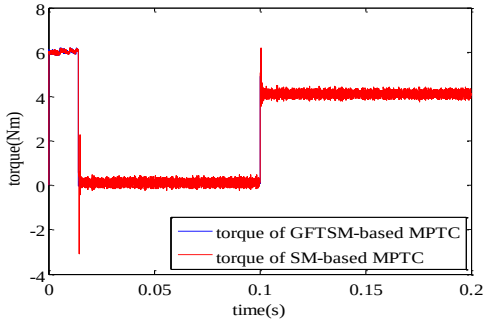

(b) Torque response

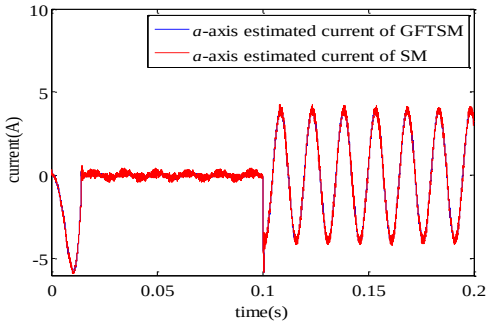

(c) *a*-axis stator current in *abc*-frame

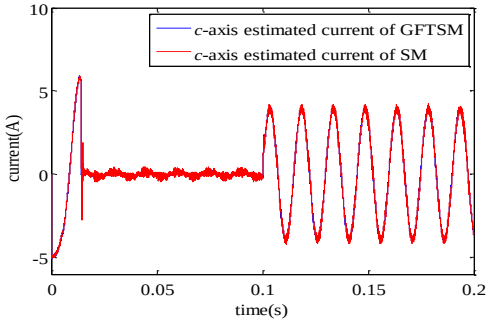

(d) *c*-axis stator current in *abc*-frame

Fig.8 The comparison of dynamic responses under the same anti-load variation ability

Figs.8(a)-8(d) show their dynamical responses in terms of speed, torque and stator currents. Fig. 8(a) shows that its speed dynamic performance is better than SM-based one's. And it can be found from Figs.8(b)-8(d) that for SM-based MPTC PMSM system, due to a switching function Sign (.) in (50), therefore its torque, estimated *a*-axis and *c*-axis currents have significantly heavy chatter. On the other hand, for GFTSM-based one, its sliding reaching law in (26) is continuous and smooth function, so the system chatter can be greatly reduced.

Summarizing above simulation experiments, we can obtain following results,

(1) The proposed adaptive observer can estimate the remaining two phase currents and stator resistance rapidly and accurately.

(2) Compared with PI-based and SM-based MPTC PMSM drive systems, GFTSM-based one has better dynamical response behavior and stronger robustness as well as smaller THD index of three-phase stator current.

V. Conclusions

This paper has put forward a novel GFTSM-based MPTC strategy for PMSM drive system with only one phase current sensor. Firstly, an adaptive observer is designed, which can be capable of concurrent online estimation of the remaining two phase currents and time-varying stator resistance rapidly and accurately. Secondly, GFTSM speed regulator is designed and its stability and convergence as well as robustness are analytically verified based on Lyapunov stability theory. Finally, the MPTC strategy is employed to reduce the torque and flux ripples. The proposed observer can be embedded into a fault resilient PMSM drive system. In case of a phase current sensor failure, the designed observer can be used as a virtual current sensor which is robust against variation of stator resistance. And the designed GFTSM controller can enhance speed regulator's robustness against variation of system parameters and external disturbance. The resultant GFTSM-based MPTC strategy can guarantee that PMSM drive system with single phase current sensor achieves not only fast response but also high-precision control performance as well as strong robustness.

Our future research topic is that considering both parameters uncertainties and unmodeled dynamics, we will employ adaptive robust method with extended state observer to reconstruct stator currents observer.

References

[1] D. Chung, S. Sul. Analysis and compensation of current measurement error in vector-controlled AC motor drives. *IEEE Trans. Industrial Application*, vol. 34, no. 2, pp. 340–345, Mar./Apr. 1998.

[2] Y. S. Jeong, S. K. Sul, E. Schulz, et al. Fault detection and fault-tolerant control of interior permanent-magnet motor drive system for electric vehicle. *IEEE Trans. Industrial Application*, vol. 41, no. 1, pp. 46-51. Jan. /Feb. 2005.

[3] J. T. Boys. Novel current sensor for PWM ac drives. In *IEE Proceedings: Electric Power Applications*, vol. 135, pp. 27-32, 1988.

[4] H. Y. Ma, K. Sun, Q. Wei, et al. Phase current reconstruction for AC motor adjustable speed drives in the over modulation method. *Journal of Tsinghua University*, vol. 50, no. 11, pp. 1757-1761, 2010.

[5] T. C. Green, B. W. Williams. Derivation of motor line-current waveforms from the DC-link current of an inverter. In *IEE Proceedings, Part B: Electric Power Applications*, vol. 136, no. 4, pp. 196-204, 1989.

[6] H. Kim, T. M. Jahns. Phase current reconstruction for AC motor drives using a DC link single current sensor and measurement voltage vectors. *IEEE Trans. on Power Electronics*, vol. 21, no. 5, pp. 1413-1419, 2006.

[7] J. Ha. Current prediction in vector controlled PWM inverters using single DC-Link current sensor. *IEEE Trans. on Industrial Electronics*, vol. 57, no. 2, pp. 716-726, 2010.

[8] K. Sun, Q. Wei, L. P. Huang, et al. An over modulation method for PWM inverter fed IPMSM drive with single current sensor. *IEEE Trans. on Industrial Electronics*, vol. 57, no. 10, pp. 3395-3404, 2010.

[9] Y. K. Gu, F. L. Ni, D. P Yang, et al. Switching state phase shift method for three phase current reconstruction with a single DC-Link current sensor. *IEEE Trans. on Industrial Electronics*, vol. 58, no. 11, pp. 5186-5194, 2011.

[10] B. Metidji, N. Taib, L. Baghli, et al. Low cost direct torque control algorithm for induction motor without AC phase current sensors. *IEEE Trans. on Power Electronics*, vol. 27, no. 9, pp. 4132-4139, 2012.

[11] Y. S. Lai, Y. K. Lin, C. W. Chen. New hybrid pulse width modulation technique to reduce current distortion and extend current reconstruction range for a three-phase inverter using only DC-link sensor. *IEEE Trans. on Power Electronics*, vol. 28, no. 3, pp. 1331-1337, 2013.

[12] H. F. Lu, X. M. Cheng, W. L. Qu, et al. A three-phase current reconstruction technique using single DC current sensor based on TSPWM. *IEEE Trans. on Power Electronics*, vol. 29, no. 3, pp.1542-1550, 2014.

[13] Y. Gu, F. Ni, D. Yang, et al. Novel method for phase current reconstruction using a single dc-link current sensor. *Electric machine and control*, vol. 13, no. 6, pp. 811-816, 2009.

[14] M. Carpaneto, P. Fazio, M. Marchesoni, et al. Dynamic performance evaluation of sensorless permanent-magnet synchronous motor drives with reduced current sensors. *IEEE Trans. on Industrial Electronics*, vol. 59, no. 12, pp. 4579-4589, 2012.

[15] Y. H. Cho, T. LaBella, J. Lai. A three-phase current reconstruction strategy with online current offset compensation using a single current sensor. *IEEE Trans. on Industrial Electronics*, vol. 59, no. 7, pp. 2924-2933, 2012.

[16] V. Verma, C. Chakraborty, S. Maiti, et al. Speed sensorless vector controlled induction motor drive using single current sensor. *IEEE Trans. on Energy Conversion*, vol. 28, no. 4, pp. 938-950, 2013.

[17] Morimoto S.,Sanada M.,Takeda Y..High-performance current-sensorless drive for PMSM and syn- RM with only low-resolution position sensor[J].*IEEE Transactions on Industry Applications*,2003,39 (3):792-801.

[18] F. R. Salmasi, T. A. Najafabadi. An adaptive observer with online rotor and stator resistance estimation for induction motors with one phase current sensor. *IEEE Trans. on Energy Conversion*, vol. 26, no. 3, pp. 959-966, 2011.

[19] Q. F. Teng, J. Y. Bai, J. G. Zhu, et al. Current sensorless model predictive torque control based on adaptive backstepping observer for PMSM drives. *WSEAS Transactions on systems*, vol. 13, pp. 187-202, 2014.

[20] J. Y. Yao, Z. X. Jiao, D. W. Ma. Adaptive robust control of DC motors with extended state observer. *IEEE Transactions on Industrial Electronics*, 2014,61 (7):3630-3637.

[21] W. C. Sun, Z. L. Zhao, H. J. Gao. Saturated adaptive robust control for active suspension systems. *IEEE Transactions on Industrial Electronics*, 2013,60 (9):3889-3896.

[22] S. Kouro, P. Cortes, R. Vargas, et al. Model predictive control—A simple and powerful method to control power converters. *IEEE Trans. on Industrial Electronics*, vol. 56, no. 6, pp. 1826-1838, 2009.

[23] H. Miranda, P. Cortes, J. I. Yuz, et al. Predictive torque control of induction machines based on state-space models. *IEEE Trans. Industry Electronics*, vol. 56,no.6, pp. 1916-1924, 2009.

[24] M. Preindl, S. Bolognani. Model predictive direct torque control with finite control set for PMSM drive systems, Part 2: field weakening operation. *IEEE Trans. on Industrial Informatics*, vol. 9, no. 2, pp. 648-657, 2013.

[25] R. P. Aguilera, P. Lezana, D. E. Quevedo. Finite-control-set model predictive control with improved steady-state performance. *IEEE Trans. on Industrial Informatics*, vol. 9, no. 2, pp. 658-667, 2013.

[26] T. Geyer. Model predictive direct torque control—Part Ⅰ: concept, algorithm, and analysis. *IEEE Trans. on Industrial Electronics*, vol. 56, no.6, pp. 1894-1905, 2009.

[27] C. E. Garcia, D. M. Prett, M. Morari. Model predictive control: theory and practice—A survey. *Automatica*, vol. 25, no. 3, pp. 335-348, 1989

[28] Q. F. Teng, J. Y. Bai, J. G. Zhu, et al. Fault tolerant model predictive control of three-phase permanent magnet synchronous motors. *WSEAS Transactions on systems*, vol. 8, no. 12, pp. 385-397, 2013.

[29] Q. F. Teng, J. Y. Bai, J. G. Zhu, et al. Sensorless model predictive torque control using sliding-mode model reference adaptive system observer for permanent magnet synchronous motor drive systems. *Control Theory & Application*, vol. 32, no. 2, pp. 150-161, 2015.

[30] Gai J T, Huang S D, Huang Q, et al. A new fuzzy active-disturbance rejection controller applied in PMSM position servo system[C]// International Conference on Electrical Machines and Systems. IEEE, 2014:2055-2059.

[31] Zhang X, Sun L, Zhao K, et al. Nonlinear Speed Control for PMSM System Using Sliding-Mode Control and Disturbance Compensation Techniques[J]. IEEE Transactions on Power Electronics. 2013, 28(3): 1358-1365

[32] Q. F. Teng, G. F. Li, J. G. Zhu, et al. Sensorless active disturbance rejection model predictive torque control using extended state observer for permanent magnet synchronous motors by three-phase four-switch inverter. *Control Theory & Application*, vol. 33, no. 5, pp. 676-684, 2016.

[33] J. Y. Yao, Z. X. Jiao, D. W. Ma. Extended-State-Observer-Based Output Feedback Nonlinear Robust Control of Hydraulic Systems with Backstepping. *IEEE Transactions on Industrial Electronics*, 2014, 61 (11):6285-6293.

[34] W. C. Sun, H. H. Pan, H. J. Gao. Filter-based Adaptive Vibration Control for Active Vehicle Suspensions with Electrohydraulic Actuators. *IEEE Transactions on Vehicular Technology*, 2016, 65 (6):4619-4626.

[35] S. H. Yu, X. H. Yu, Z. H. Man. Robust global terminal sliding mode control of SISO nonlinear uncertain system [A]. Proceedings of 39th IEEE Conference on decision and control, Sydney, Australia, December, 2000:2198-2203.

[36] X. H. Yu, Z. H. Man. Fast terminal sliding mode control design for nonlinear dynamical systems. *IEEE Trans. on circuits and systems* —Ⅰ: fundamental theory and applications, vol. 49, no. 2, pp.261-264, 2002.